

MAFNET : MULTI-FREQUENCY ADAPTIVE FUSION NETWORK FOR REAL-TIME STEREO MATCHING

Ao Xu², Rujin Zhao^{3,6}, Xiong Xu^{1,2,4,5,}, Boceng Huang¹, Yujia Jia², Hongfeng Long³, Fuxuan Chen¹, Zilong Cao¹, Fangyuan Chen¹*

¹College of Surveying and Geo-Informatics, Tongji University, Shanghai, China

²Shanghai Research Institute for Intelligent Autonomous Systems, Tongji University, Shanghai, China

³Institute of Optics and Electronics of Chinese Academy of Sciences, Chengdu 610209, China

⁴Shanghai Integrated Innovation Center for Manned Lunar Exploration, Shanghai, China

⁵Shanghai Key Laboratory for Planetary Mapping and Remote Sensing for Deep Space Exploration, Shanghai, China

⁶University of Chinese Academy of Sciences, Beijing 100049, China

ABSTRACT

Existing stereo matching networks typically rely on either cost-volume construction based on 3D convolutions or deformation methods based on iterative optimization. The former incurs significant computational overhead during cost aggregation, whereas the latter often lacks the ability to model non-local contextual information. These methods exhibit poor compatibility on resource-constrained mobile devices, limiting their deployment in real-time applications. To address this, we propose a Multi-frequency Adaptive Fusion Network (MAFNet), which can produce high-quality disparity maps using only efficient 2D convolutions. Specifically, we design an adaptive frequency-domain filtering attention module that decomposes the full cost volume into high-frequency and low-frequency volumes, performing frequency-aware feature aggregation separately. Subsequently, we introduce a Linformer-based low-rank attention mechanism to adaptively fuse high- and low-frequency information, yielding more robust disparity estimation. Extensive experiments demonstrate that the proposed MAFNet significantly outperforms existing real-time methods on public datasets such as Scene Flow and KITTI 2015, showing a favorable balance between accuracy and real-time performance.

Index Terms— Stereo Matching, 3D Vision, Real-Time Depth Estimation

1. INTRODUCTION

With the advent of autonomous driving, drone inspection, smart manufacturing, augmented reality, and medical robotics, acquiring accurate 3D structural information has

become essential for intelligent perception systems [1–3]. Stereo matching, which estimates scene depth by establishing pixel correspondences between rectified image pairs under geometric constraints, is a key component of 3D vision [4]. Leveraging deep learning, end-to-end stereo networks [5–8] have achieved state-of-the-art results on benchmarks such as Scene Flow [9] and KITTI [10], driving the adoption of 3D vision across research and industry.

Recent studies have extensively explored cost-volume construction and representation to improve stereo matching [11, 12]. Representative methods include GwcNet [11], which computes group-wise correlations to form more discriminative volumes; ACVNet [13], which introduces attention mechanisms to convert correlation volumes into attention weights for finer filtering; and PCWNet [14], which combines pyramidal structures with deformable volumes for enhanced multi-scale modeling. While these approaches significantly boost accuracy, their reliance on high-resolution volumes and large-scale 3D convolutions incurs heavy computational and memory costs, hindering real-time deployment on resource-constrained mobile or embedded platforms.

To improve efficiency, subsequent studies have introduced lightweight strategies such as constructing lower-resolution cost volumes, adopting sparse disparity searches, and employing lightweight aggregation networks like StereoNet [15], DeepPruner [16], and Fast-ACVNet [17]. While these methods achieve faster inference on high-end GPUs, they still depend on extensive 3D convolutions or complex deformable operations, limiting deployment on mobile platforms. Another line of work replaces 3D with 2D convolutions for cost aggregation, e.g., AANet [18] uses deformable convolutions for adaptive aggregation, and MobileStereoNet-2D [19] integrates lightweight MobileNet

*Corresponding author: xvxiang@tongji.edu.cn

modules. Although these approaches improve efficiency, they remain prone to errors in blurred textures, textureless regions, and fine edges, leading to noticeable detail loss.

To overcome these limitations, MAFNet introduces an adaptive frequency-domain attention to explicitly separate high-frequency details from low-frequency regions and a Linformer-based fusion module for lightweight, dynamic aggregation. This design retains the efficiency of 2D convolutions while strengthening the modeling of complex textures and edges, thus achieving a better trade-off between real-time performance and accuracy and making the network well suited for edge or mobile deployment.

2. RELATED WORKS

Deep stereo networks can be broadly categorized into cost-volume aggregation and iterative refinement. Cost-volume methods, such as PSMNet, GwcNet, and ACVNet, achieve high accuracy by constructing 4D cost volumes and aggregating features with 3D convolutions, which improves both matching precision and geometric consistency. However, the heavy computational and memory requirements of 3D convolutions hinder real-time deployment, particularly on resource-constrained devices.

Iterative refinement methods, including RAFT-Stereo [20] and IGEV-Stereo, avoid expensive 3D aggregation by repeatedly updating disparities over correlation pyramids. This approach enhances edge and fine-detail accuracy but involves multiple update steps, leading to slower inference.

To alleviate computational cost, lightweight 2D aggregation networks such as AANet and MobileStereoNet-2D replace 3D convolutions with deformable 2D convolutions or efficient backbone modules. While these designs improve efficiency and real-time applicability, they remain challenged by textureless regions, blurred textures, and fine edges, often resulting in unstable matches.

3. METHODOLOGY

3.1. Model Architecture

As shown in Fig. 1, our network takes a pair of rectified images as input and first extracts multi-scale high-dimensional features using a weight-sharing MobileViT backbone. Specifically, feature maps are obtained at four scales: 1/4, 1/8, 1/16, and 1/32 of the original resolution. Starting from the 1/32-resolution features, we progressively upsample to 1/4 resolution via transposed convolutions with a 4×4 kernel and stride 2, producing multi-scale features $\{f_l, f_r\}$ for the left and right images, with three key scales (1/4, 1/8, 1/16) retained. The multi-scale features of the left image are fed into an adaptive frequency-domain filtering attention module to generate frequency-aware spatial weights, while the 1/4-resolution features of both images are used to construct the cost volume.

Under the adaptive frequency-domain filtering attention, multi-scale features are separated into high- and low-frequency components: the former captures edges and fine details, while the latter preserves the structure of smooth or textureless regions. Based on this separation, we construct high- and low-frequency cost volumes from the corresponding features and feed them into a high-low frequency adaptive fusion module for efficient feature aggregation. Finally, a softmax is applied to the aggregated cost volume, and disparity regression is performed to generate the final disparity map.

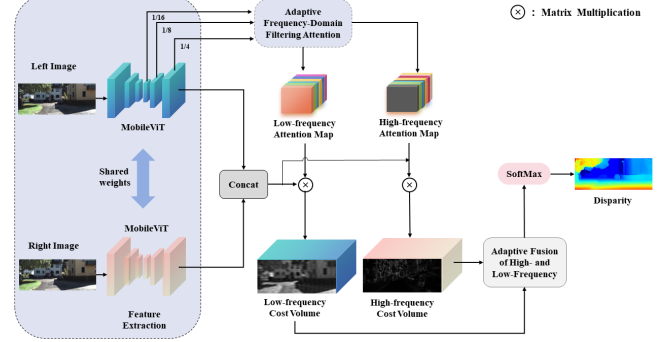


Fig. 1. Overview of our proposed MAFNet.

3.2. Adaptive Frequency-Domain Filtering Attention

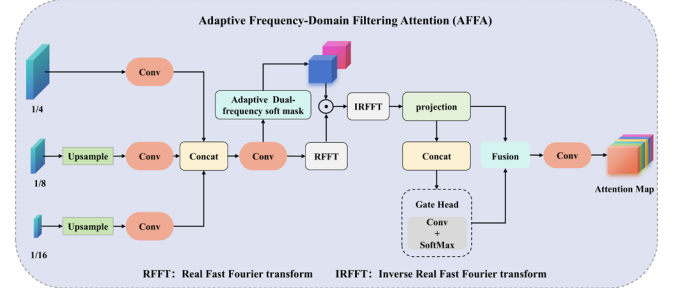


Fig. 2. AFFA Structure Diagram.

High-frequency image components mainly encode fine details and edges, while low-frequency components capture global structures and textureless regions. To leverage these complementary features, we propose an adaptive frequency-domain filtering attention module. The module first decomposes feature maps in the frequency domain to obtain high- and low-frequency subbands. A learnable spatial gating mechanism is then applied to dynamically generate pixel-wise fusion weights for the two subbands. The resulting attention maps adaptively distinguish frequency characteristics across different regions, effectively enhancing edge fidelity and improving matching stability in textureless areas.

As illustrated in Fig. 2, given a feature map $X \in \mathbb{R}^{B \times C \times H \times W}$, we first compute its 2D Fast Fourier Transform (RFFT) to obtain the frequency-domain representation:

$$F(X) = RFFT(X), F(X) \in \mathbb{C}^{B \times C \times H \times W} \quad (1)$$

In the frequency plane, the low-frequency components are concentrated near the center while the high-frequency

components are distributed toward the edges. We introduce learnable thresholds τ_l and τ_h to adaptively separate the bands and construct soft masks as:

$$M_{low}(u, v) = \sigma\left(\frac{\tau_l - r(u, v)}{\gamma}\right) \quad (2)$$

$$M_{high}(u, v) = \sigma\left(\frac{r(u, v) - \tau_h}{\gamma}\right) \quad (3)$$

where, $r(u, v)$ denotes the normalized radius from a frequency-domain point to the center, σ is the sigmoid function, and γ is the temperature parameter used to control the smoothness of the soft threshold. Thus, the high- and low-frequency decomposition is obtained:

$$X_{low} = IRFFT(F(X) \odot M_{low}), X_{high} = IRFFT(F(X) \odot M_{high}) \quad (4)$$

To avoid the constraints introduced by fixed frequency band division, we propose a spatially adaptive gating mechanism. Specifically, the high- and low-frequency features are first concatenated:

$$Z = \text{Concat}[X_{low}, X_{high}] \in \mathbb{R}^{B \times 2C \times H \times W} \quad (5)$$

Then, pixel-level weights are obtained via a 1×1 convolution:

$$G = \text{SoftMax}(\text{Conv}_{1 \times 1}(Z)) \in \mathbb{R}^{B \times 2 \times H \times W} \quad (6)$$

The fused feature is given by:

$$X_f = G_{low} \odot X_{low} + G_{high} \odot X_{high} \quad (7)$$

Finally, an attention map is generated through convolution followed by a sigmoid function:

$$A = \sigma(\text{Conv}(X_f)) \quad (8)$$

3.3. Adaptive Fusion of High- and Low- Frequency

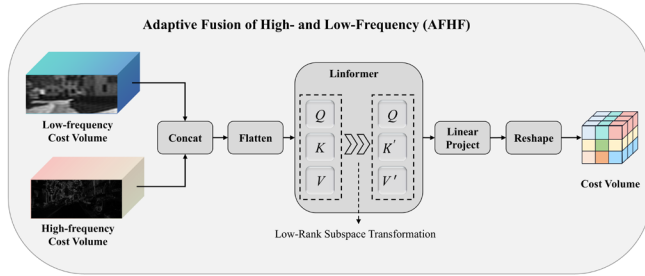


Fig. 3. AFHF Structure Diagram.

The high-frequency feature and low-frequency feature respectively capture detailed edges and smooth regions, and they are complementary in stereo matching. Simply using element-wise addition or multiplication for fusion often fails to adaptively adjust their contributions across different regions, resulting in insufficient feature aggregation. To address this, we introduce a Linformer-based adaptive fusion module, which employs low-rank attention mapping to achieve efficient and dynamic feature fusion.

As shown in Fig. 3, given the input high-frequency cost volume $CV_{high} \in \mathbb{R}^{B \times D \times H \times W}$ and low-frequency cost volume $CV_{low} \in \mathbb{R}^{B \times D \times H \times W}$, we first concatenate them to obtain:

$$CV_{all} \in \text{Concat}(CV_{high}, CV_{low}) \in \mathbb{R}^{B \times 2D \times H \times W} \quad (9)$$

It is then flattened into a sequential representation:

$$X = \text{Reshape}(CV_{all}) \in \mathbb{R}^{B \times N \times 2D}, N = H \times W \quad (10)$$

The standard self-attention is defined as:

$$\text{Att}(Q, K, V) = \text{SoftMax}\left(\frac{QK^T}{\sqrt{d}}\right)V \quad (11)$$

where $Q, K, V \in \mathbb{R}^{N \times d}$, with a computational complexity of $O(N^2)$. In Linformer, the key K and value V are projected into a low-rank subspace:

$$K' = EK, V' = FV, (E, F) \in \mathbb{R}^{k \times N}, k \ll N \quad (12)$$

The attention computation is given by:

$$\text{LinAtt}(Q, K, V) = \text{SoftMax}\left(\frac{QK'^T}{\sqrt{d}}\right)V' \quad (13)$$

The complexity is reduced to $O(N \cdot k)$. Through the low-rank approximation, the model can significantly reduce computational cost while maintaining representational capacity. Finally, we use a linear projection to map the output back to $\mathbb{R}^{B \times N \times \tilde{D}}$ and reshape it into the fused feature:

$$F_{fused} = \text{Reshape}(\text{LinAtt}(X)) \in \mathbb{R}^{B \times D \times H \times W} \quad (14)$$

3.4. Loss Function

The entire network is trained in a supervised end-to-end manner, and the final loss function is defined as:

$$L = \lambda_0 L_{1 \text{ smooth}}(D_0 - D_{gt}) + \lambda_1 L_{1 \text{ smooth}}(D_1 - D_{gt}) \quad (15)$$

where D_{gt} denotes the ground-truth disparity map, and $L_{1 \text{ smooth}}$ represents the smooth L1 loss. D_0 denotes the full-scale disparity, while D_1 denotes the disparity at one-quarter of the original image scale.

4. EXPERIMENT

4.1. Implementation Details and Dataset

The proposed MAFNet model was implemented using PyTorch, and experiments were carried out on the Scene Flow, KITTI 2012, and KITTI 2015 datasets. All experiments were conducted on an NVIDIA RTX 5090 GPU. We employed the AdamW [21] optimizer combined with a one-cycle learning rate scheduler with warm-up, setting the maximum learning rate to $8e-4$. The weights in the loss function were configured as $\lambda_0 = 0.3$ and $\lambda_1 = 1.0$. During training, we initially pre-trained on the Scene Flow dataset for 200k steps with a batch size of 16 to adequately learn the distribution of large-scale synthetic data. The resulting model was then fine-tuned for 50k steps on the mixed KITTI 2012 and KITTI 2015 training sets to improve performance in real-world environments. During training, each input image was randomly cropped to a resolution of 256×512 .

4.2. Ablation Study

Comprehensive ablation studies were carried out on Scene Flow and KITTI 2015 to verify the effectiveness of the proposed approach, with the ablation results for Scene Flow

presented in Table 1 and those for KITTI 2015 presented in Table 2.

The Baseline, a single-branch 2D convolutional aggregation network, achieves 0.66 EPE and 2.94% Bad 3.0 on Scene Flow, and 2.17% D1-all on KITTI 2015. Method (1) adds the AFFA module, reducing EPE to 0.62, Bad 3.0 to 2.73%, and D1-all to 1.96%, showing that adaptive frequency-domain filtering better captures high-frequency details while preserving low-frequency regions. Method (2), which adds only the AFHF module, achieves 0.63 EPE, 2.79% Bad 3.0, and 2.01% D1-all, indicating that adaptive fusion of high- and low-frequency features improves the complementarity of aggregated features with minimal parameter increase. Method (3) combines both modules, further reducing EPE to 0.58, Bad 3.0 to 2.56%, and D1-all to 1.82%, demonstrating that their synergy enables more precise separation and fusion of cost volumes across frequencies, significantly enhancing matching accuracy in edge and textureless regions while keeping parameter counts nearly unchanged.

TABLE I

RESULTS OF ABLATION EXPERIMENT ON THE SCENE FLOW DATASET

Method	AFFA	AFHF	EPE (px)	Bad 3.0 (%)	Param (M)
Baseline			0.66	2.94	10.346
Method(1)	√		0.62	2.73	10.358
Method(2)		√	0.63	2.79	10.350
Method(3)	√	√	0.58	2.56	10.363

TABLE II

RESULTS OF ABLATION EXPERIMENT ON THE KITTI 2015 DATASET

Method	AFFA	AFHF	D1-bg	D1-fg	D1-all
Baseline			1.81	3.38	2.17
Method(1)	√		1.67	3.12	1.96
Method(2)		√	1.70	3.15	2.01
Method(3)	√	√	1.58	2.97	1.82

4.3. Comparisons with State-of-the-Art Methods

A systematic comparison with existing real-time methods was carried out on KITTI 2015. For all compared methods, the implementation environments and parameter settings strictly followed those in the original papers, with the experimental results presented in Table 3.

Table 3 reports the KITTI-2015 results. Our MAFNet attains the best accuracy among all lightweight methods without 3D convolutions, reaching 1.82% D1-all, surpassing HITNet (1.98%), Fast-ACVNet+ (2.01%), and MobileStereoNet-2D (2.83%). It also yields the lowest D1-fg error (2.97%), evidencing superior robustness on foreground details and edges. Moreover, MAFNet requires only 39.40 G FLOPs, far below AANet+ (152.86 G), DeepPruner-Fast (219.12 G) and Fast-ACVNet+ (93.08 G), thus markedly cutting computation while preserving accuracy. These results

confirm that our adaptive frequency-domain filtering and high-low frequency fusion strike a favorable trade-off between accuracy and efficiency, facilitating deployment on resource-limited or real-time platforms.

TABLE III

COMPARISON WITH STATE-OF-THE-ART METHODS ON THE KITTI 2015 DATASET

Method	D1- bg	D1- fg	D1- all	FLOPs (G)	Param (M)
CoEx [22]	1.79	3.82	2.13	53.39	2.72
AANet+ [18]	1.65	3.96	2.03	152.86	2.97
DeepPruner-Fast [16]	2.32	3.91	2.59	219.12	7.47
Fast-ACVNet [17]	1.82	3.93	2.17	79.34	3.08
Fast-ACVNet+ [17]	1.70	3.53	2.01	93.08	3.20
HITNet [23]	1.74	3.20	1.98	50.23	0.42
MobileStereoNet-2D [19]	2.49	4.53	2.83	128.84	2.23
MAFNet(ours)	1.58	2.97	1.82	39.40	10.36

Fig. 4 shows the visual comparison of our method with MobileStereoNet-2D, confirming the effectiveness of the proposed method.

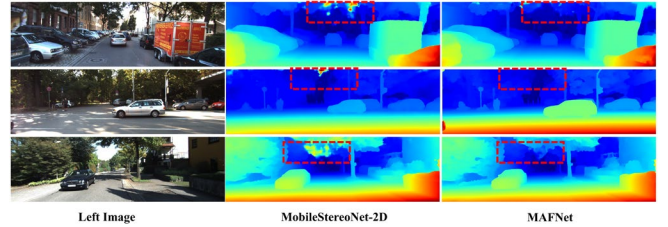


Fig. 4. Visualization results on the KITTI 2012 and 2015 test sets.

5. CONCLUSION

In this work, we introduced MAFNet, a novel stereo matching network that effectively balances accuracy and efficiency for real-time applications on resource-constrained devices. By leveraging an adaptive frequency-domain filtering attention module and a Linformer-based low-rank fusion mechanism, MAFNet can separately process high- and low-frequency information and integrate them for robust disparity estimation, while avoiding the computational burden of 3D convolutions. Extensive experiments on Scene Flow and KITTI 2015 benchmarks validate that MAFNet consistently outperforms existing real-time stereo matching methods, achieving superior accuracy with reduced computational cost. This demonstrates the potential of frequency-aware feature aggregation and low-rank attention in designing lightweight yet high-performance stereo networks, providing a promising solution for real-world mobile and embedded vision applications.

5. ACKNOWLEDGMENT

This work was partly supported by the National Natural Science Foundation of China under Grant 42471450, 42221002, the Natural Science Foundation of Shanghai under Grant 24ZR1471200 and the Fundamental Research Funds for the Central Universities.

REFERENCES

- [1]. Geiger A, Lenz P, Stiller C, et al. Vision meets robotics: The kitti dataset[J]. *The international journal of robotics research*, 2013, 32(11): 1231-1237.
- [2]. Zhang H, Liu L Z, Xie H, et al. Deep learning-based robot vision: High-end tools for smart manufacturing[J]. *IEEE Instrumentation & Measurement Magazine*, 2022, 25(2): 27-35.
- [3]. Xia W, Chen E C S, Pautler S, et al. A robust edge-preserving stereo matching method for laparoscopic images[J]. *IEEE Transactions on Medical Imaging*, 2022, 41(7): 1651-1664.
- [4]. Liu C W, Chen Q, Fan R. Playing to Vision Foundation Model's Strengths in Stereo Matching[J]. *IEEE Transactions on Intelligent Vehicles*, 2024.
- [5]. Wen B, Trepte M, Aribido J, et al. Foundationstereo: Zero-shot stereo matching[C]//*Proceedings of the Computer Vision and Pattern Recognition Conference*. 2025: 5249-5260.
- [6]. Xu H, Zhang J, Cai J, et al. Unifying flow, stereo and depth estimation[J]. *IEEE Transactions on Pattern Analysis and Machine Intelligence*, 2023, 45(11): 13941-13958.
- [7]. Xu G, Liu J, Wang X, et al. BANet: Bilateral Aggregation Network for Mobile Stereo Matching[J]. *arXiv preprint arXiv:2503.03259*, 2025.
- [8]. Xu G, Wang X, Ding X, et al. Iterative geometry encoding volume for stereo matching[C]//*Proceedings of the IEEE/CVF conference on computer vision and pattern recognition*. 2023: 21919-21928.
- [9]. Mayer N, Ilg E, Hausser P, et al. A large dataset to train convolutional networks for disparity, optical flow, and scene flow estimation[C]//*Proceedings of the IEEE conference on computer vision and pattern recognition*. 2016: 4040-4048.
- [10]. Menze M, Geiger A. Object scene flow for autonomous vehicles[C]//*Proceedings of the IEEE conference on computer vision and pattern recognition*. 2015: 3061-3070.
- [11]. Guo X, Yang K, Yang W, et al. Group-wise correlation stereo network[C]//*Proceedings of the IEEE/CVF conference on computer vision and pattern recognition*. 2019: 3273-3282.
- [12]. Xu G, Wang X, Zhang Z, et al. Igev++: Iterative multi-range geometry encoding volumes for stereo matching[J]. *IEEE Transactions on Pattern Analysis and Machine Intelligence*, 2025.
- [13]. Xu G, Cheng J, Guo P, et al. Attention concatenation volume for accurate and efficient stereo matching[C]//*Proceedings of the IEEE/CVF conference on computer vision and pattern recognition*. 2022: 12981-12990.
- [14]. Shen Z, Dai Y, Song X, et al. Pcw-net: Pyramid combination and warping cost volume for stereo matching[C]//*European conference on computer vision*. Cham: Springer Nature Switzerland, 2022: 280-297.
- [15]. Khamis S, Fanello S, Rhemann C, et al. Stereonet: Guided hierarchical refinement for real-time edge-aware depth prediction[C]//*Proceedings of the European conference on computer vision (ECCV)*. 2018: 573-590.
- [16]. Duggal S, Wang S, Ma W C, et al. Deeppruner: Learning efficient stereo matching via differentiable patchmatch[C]//*Proceedings of the IEEE/CVF international conference on computer vision*. 2019: 4384-4393.
- [17]. Xu G, Wang Y, Cheng J, et al. Accurate and efficient stereo matching via attention concatenation volume[J]. *IEEE Transactions on Pattern Analysis and Machine Intelligence*, 2023, 46(4): 2461-2474.
- [18]. Xu H, Zhang J. Aanet: Adaptive aggregation network for efficient stereo matching[C]//*Proceedings of the IEEE/CVF conference on computer vision and pattern recognition*. 2020: 1959-1968.
- [19]. Shamsafar F, Woerz S, Rahim R, et al. Mobilestereonet: Towards lightweight deep networks for stereo matching[C]//*Proceedings of the IEEE/CVF winter conference on applications of computer vision*. 2022: 2417-2426.
- [20]. Lipson L, Teed Z, Deng J. Raft-stereo: Multilevel recurrent field transforms for stereo matching[C]//*2021 International Conference on 3D Vision (3DV)*. IEEE, 2021: 218-227.
- [21]. Loshchilov I, Hutter F. Decoupled weight decay regularization[J]. *arXiv preprint arXiv:1711.05101*, 2017.
- [22]. Bangunharcana A, Cho J W, Lee S, et al. Correlate-and-excite: Real-time stereo matching via guided cost volume excitation[C]//*2021 IEEE/RSJ International Conference on Intelligent Robots and Systems (IROS)*. IEEE, 2021: 3542-3548.
- [23]. Tankovich V, Hane C, Zhang Y, et al. Hitnet: Hierarchical iterative tile refinement network for real-time stereo matching[C]//*Proceedings of the IEEE/CVF conference on computer vision and pattern recognition*. 2021: 14362-14372.